# This is a post-referee draft, the final version is available at

https://doi.org/10.1016/j.actamat.2021.117007

Microstructure and Phase Composition Evolution of Silicon-Hafnia Feedstock during Plasma Spraying and Following Cyclic Oxidation

Emine Bakana\*, Yoo Jung Sohna, Robert Vaßena

#### Abstract

In this work, silicon–hafnia (Si-HfO₂, 80/20 mol. %) feedstock was plasma sprayed for Environmental Barrier Coating bond coat application. In the as-sprayed coating, hafnium disilicide (HfSi₂), HfO₂ tetragonal (t), and cubic (c) phases with a total volume of ~20% were detected together with Si and HfO₂ monoclinic (m). The temperature-dependent evolution of these phases was analyzed and paired with microstructural observations. It was found that above 700°C, HfSi₂ oxidizes and HfO₂ (t) and (c) transforms into (m) polymorph. Up to this temperature, as-sprayed coating showed a non-linear expansion behavior. Estimated volume expansion at ~750°C was 3.6% based on dilatometry measurement. The primary and secondary mechanisms leading to the expansion in the coating were identified as oxidation of HfSi₂ and polymorphic phase transitions in HfO₂, respectively. As a consequence of the volume expansion, the coating was extensively cracked during cyclic oxidation and hence not protective anymore. After 100 h at 1300°C, the volume fraction of oxidation product SiO₂ was significant in the coating (0.34), while HfO₂ was largely consumed (0.1) in the formation of HfSiO₄ (0.56). This result suggested that reversible α↔β phase transitions in SiO₂-cristobalite could be another factor contributing to the cracking in the coating during cyclic oxidation.

<sup>&</sup>lt;sup>a</sup> Forschungszentrum Jülich GmbH, Institute of Energy and Climate Research, Materials Synthesis and Processing (IEK-1), 52425 Jülich, Germany

<sup>\*</sup>Corresponding Author. Forschungszentrum Jülich GmbH, Institute of Energy and Climate Research, Materials Synthesis and Processing (IEK-1), 52425 Jülich, Germany, Tel: +49 2461 61 2785; Fax: +49 2461 61 2455, e-mail: e.bakan@fz-juelich.de.

**Keywords**: Ceramic matrix composite, Environmental Barrier Coating, silicon, metastable phases, plasma spraying

## 1. Introduction

Environmental barrier coatings (EBCs) are used to shield SiC/SiC ceramic matrix composite (CMCs) components from water vapor-containing atmosphere in the hot sections of gas turbine engines [1]. In the engine atmosphere, volatilization of protective SiO<sub>2</sub> scale growing on SiC occurs and results in rapid CMC surface recession [2, 3]. Therefore, EBCs have been developed over the two last decades to protect CMCs from surface recession, oxidation as well as CMAS degradation [4-6]. An EBC system consists of a Si bond coat and oxide-based volatilization barrier such as rare-earth silicates, barium-strontium-aluminum silicates, and mullite [7-9]. The Si bond coat forms a sacrificial oxidation layer akin to an aluminum-rich metallic bond coat in thermal barrier coatings. During service, the oxidizers (mainly O<sub>2</sub> (g), and H<sub>2</sub>O (g)) permeate through the volatilization barrier and react with the Si bond coat to form a passivating SiO<sub>2</sub> scale. The SiO<sub>2</sub> growing on Si is a dense, slow-growing oxide with good adhesion, unlike the porous oxidation layer that grows on SiC due to the emission of additional reaction products (e.g. CO (g)) [10]. Therefore, the use of the Si bond coat is required despite its low melting point (1414 °C), which significantly reduces the maximum temperature capability of the coating system.

The dense SiO<sub>2</sub> layer thermally growing on the Si bond coat was nevertheless related to the degradation of the EBC system [11]. Richards et al. detected  $\alpha$ -cristobalite within the silica scale at room temperature (RT) and suggested that thermally grown amorphous SiO<sub>2</sub> scale crystallizes into the  $\beta$ -cristobalite at elevated temperatures. Upon cooling, the  $\beta$ -cristobalite transforms to the low-temperature phase  $\alpha$ -cristobalite at ~220-270 °C, which is accompanied by ~5% volume contraction [12]. The reversible  $\alpha \leftrightarrow \beta$  transformation gives rise to extensive cracking in the oxide layer during the thermal cycling process and eventually leads to the

spallation of the layer. For that reason, advanced EBC bond coats are required both to increase the high-temperature capability of the coating system and to avoid the formation of deleterious phases for longevity.

HfO<sub>2</sub>-doped Si bond coat is a concept for this purpose developed by NASA. NASA claims that by HfO<sub>2</sub> addition into Si, high-temperature capability and creep properties of the bond coat can be improved [13]. In this system, Si acts as an oxygen gatherer and after the formation of SiO<sub>2</sub>, HfO<sub>2</sub> reacts with it at elevated temperatures to form HfSiO<sub>4</sub> (hafnon) phase. Hafnon is a high-temperature stable phase with a well matching coefficient of thermal expansion (3.11-5.97 x10<sup>-6</sup> K<sup>-1</sup> [14]) to that of Si (4.1x10<sup>-6</sup> K<sup>-1</sup>). It is expected that, if the hafnon formation is sufficiently rapid at the temperatures of interest for EBC application, by consumption of SiO<sub>2</sub> in the hafnon formation reaction, SiO<sub>2</sub> induced coating delamination can be avoided. Nevertheless, it is apparent that the maximum temperature capability of the Si-HfO<sub>2</sub> system is still limited to 1414 °C since metallic Si melts at this temperature or above as shown by Harder's work [13]. In that study, the Si-HfO<sub>2</sub> coatings were deposited using plasma-sprayed physical vapor deposition (PS-PVD) process and the high-temperature oxidation performance of the coatings was investigated. It was observed that after 100 h exposure in the air or 31 h exposure in water vapor at 1371 °C, Si in the coatings was completely oxidized, and afterward, oxidation continued at the SiC-bond coat interface.

The Si-HfO<sub>2</sub> system with low (36 mol.%) and high (60 mol.%) hafnia additions were also studied by Anton et al. [15] using the magnetron sputtering process. This study showed that the oxidation rate of columnar structured Si-HfO<sub>2</sub> coating is significantly dependent on hafnia content, i.e. high hafnia system has a higher oxidation rate because the network of hafnia particles within the coating allows fast diffusion of oxygen. It was also reported that low hafnia doped coating had the same oxidation rate as that of a pure Si bond coat at 1250 °C in air.

In this work, the phase composition and microstructure of the Si-HfO<sub>2</sub> bond coat deposited from the molten particle state using an atmospheric plasma spray (APS) process were investigated. APS is a widely used method for the deposition of protective coatings on gas turbine engine components and is less costly than the deposition methods with controlled atmosphere chambers. To the best of our knowledge, there is no reported study of APS deposited Si-HfO<sub>2</sub> bond coats for EBC application. The deposited coatings were investigated in terms of phase composition in the as-sprayed state and after oxidation. Additionally, thermal expansion and the cyclic oxidation performance of the Si-HfO<sub>2</sub> coating between room temperature and 1300 °C in air was tested.

## 2. Materials and Method

A Si-HfO<sub>2</sub> powder (Oerlikon Metco Inc. Westbury, NY, USA) with the particle sizes of  $d_{10}$ =19 µm,  $d_{50}$ =40 µm, and  $d_{90}$ =65 µm (laser diffraction, LA-950-V2, Horiba Ltd., Tokyo, Japan) was used for thermal spraying. According to chemical analysis results (inductively coupled plasma optical emission spectroscopy, iCAP 7600, Thermo Fischer Scientific GmbH, Kleve, Germany), the powder contains 33 wt.%±0.12 wt.% Si, 56 wt.%±0.3 wt.% Hf with the rest being oxygen (~80 mol % Si/ 20 mol % HfO<sub>2</sub>). The morphology of the powder is shown in Fig. 1a and EDS spectra (energy-dispersive X-ray spectroscopy) taken from the particles are shown in Fig. 1b-c. Accordingly, the spherical particles are HfO<sub>2</sub>; the irregular shape particles with the darker contrast are Si-rich. As shown in Fig. 1d, spherical HfO<sub>2</sub> particles are also packed with Si particles. The phase composition of the powder will be further discussed in the results section. Finally, Fig. 1e shows a high magnification surface image of an HfO<sub>2</sub> particle, wherein primary hafnia particles with a size of ~100 nm can be seen. The Si powder (Oerlikon Metco Inc. Westbury, NY, USA) used for the deposition of the baseline Si bond coat had a fused and crushed microstructure and particle sizes of  $d_{10}$ =28 µm,  $d_{50}$ =40 µm, and  $d_{90}$ =59 µm.

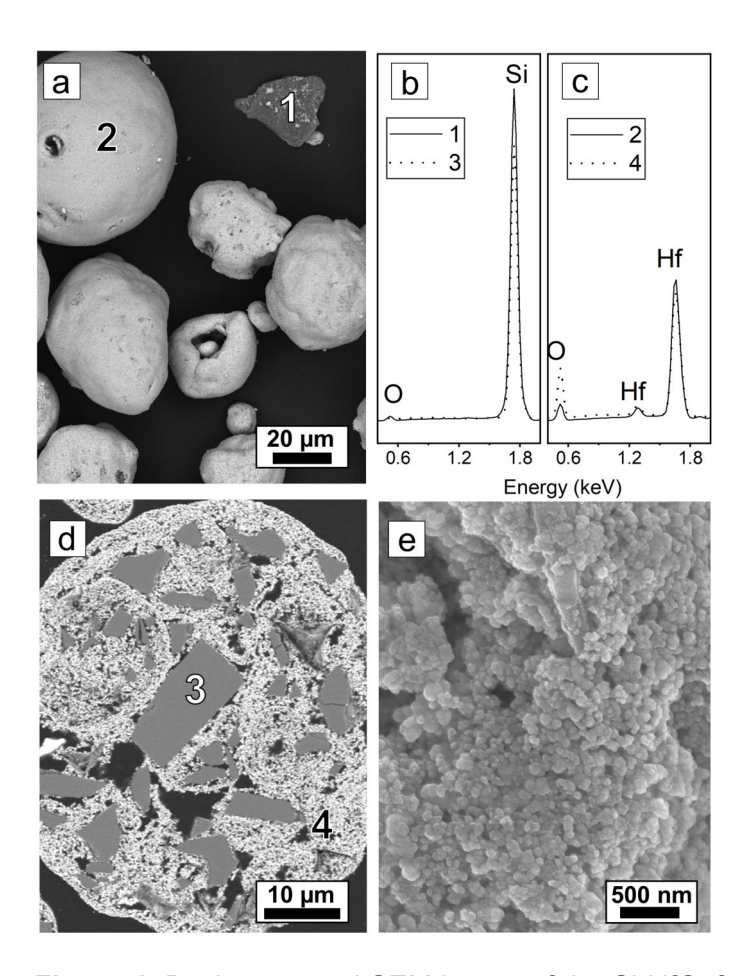


**Figure 1**: Back-scattered SEM image of the Si-HfO<sub>2</sub> feedstock (a), EDS spectra of points 1–4 (b-c) shown in (a, d), cross-section image of an HfO<sub>2</sub> particle (d), high magnification surface image of an agglomerated HfO<sub>2</sub> particle (e).

Two different kinds of samples were prepared for the investigation using a TriplexPro<sup>™</sup> -210 spray gun (Oerlikon Metco Inc. Westbury, NY, USA). Details of the spray parameters are given in Table 1. Intending to achieve minimum but sufficient thermal heat transfer as well as high momentum transfer to the particles to minimize oxidation of silicon during deposition, no auxiliary plasma gases were used and a nozzle with a small diameter (6.5 mm) was selected. The coatings with ~1 mm thickness were deposited from both Si and Si-HfO₂ feedstock on NaCl coated stainless steel substrates. By dissolving the salt layer in water, freestanding coatings were obtained and cut into rectangular shape samples (25x5 mm²) for dilatometry measurements. The measurements were performed in air with a Netzsch DIL 402C dilatometer (Netzsch GmbH, Selb, Germany) between RT and 1200 °C using a heating rate of 3 K/min.

Secondly, a thin coating (~150 µm) was deposited from Si-HfO<sub>2</sub> feedstock using the same spray parameters on SiC/SiC coupon (25x25x3 mm) (manufacturing details of SiC/SiC material are available elsewhere [16]) for cyclic oxidation test. The cycling was done in a box furnace between RT and 1300 °C, using a heating/cooling rate of 10 K/min. The high-temperature dwell time was 10 h at each cycle and the total number of cycles was 10.

**Table 1**: Atmospheric plasma spray parameters for deposition of Si and Si-HfO<sub>2</sub> bond coat.

Parameters	Setting
Plasma Gas Composition	50 slpm Ar
Spray Current	450 A
Torch Power	40 kW
Spray Distance	100 mm
Robot Velocity	500 mm/s

The microstructure of the samples was examined by scanning electron microscopy (SEM, ULTRA 55, Carl Zeiss NTS GmbH, Oberkochen, Germany) in the backscattered electron (BSE) mode and EDS (Octane Puls, EDAX, Ametek GmbH, Meerbusch, Germany) using an accelerating voltage of 8 kV. X-ray diffraction (XRD) was performed using a Bruker D4 Endeavor diffractometer (Bruker AXS GmbH, Karlsruhe, Germany) in Bragg-Brentano geometry using a Cu Kα radiation. High-temperature XRD (HT-XRD) was performed at the Empyrean diffractometer (Malvern Panalytical GmbH, Almelo, Netherlands). It was set up with Cu Κα source and Bragg-Brentano geometry combined with primary and secondary fixed divergence and soller slits. The measurements were performed in air between RT and 1200 °C with 100 K steps. The dwell time at each temperature step was ~ 40 min. An environmental heating chamber HTK1200N (Anton Paar GmbH, Graz, Austria), which allows a homogenous temperature distribution during the data collection, was used for the HT-XRD measurements. Nevertheless it should be noted here that all XRD data related to coatings were collected from the surface of coated coupons in this work therefore observed phase transformation or oxidation rates reflect the surface conditions. Quantitative phase analysis of XRD patterns for the composition analysis and determination of the crystal lattice parameters were carried out with

the use of TOPAS V4 Software (Bruker AXS GmbH, Karlsruhe, Germany). In the quantitative phase analysis, the Brindley method implemented in TOPAS was used to test the effect of different absorption coefficients of the phases on the results [17].

### 3. Results and Discussion

## 3.1. Phase composition—feedstock and as-sprayed coating

Fig. 2 presents XRD-patterns of the Si-HfO<sub>2</sub> feedstock and the as-sprayed coating. The XRDpattern of the feedstock was indexed with HfO<sub>2</sub> (monoclinic (m) and tetragonal (t), ICSD 27313, and ICSD 173966, respectively) and Si (cubic, ICSD ICSD 51688) phases. Quantitative phase analysis of the powder was performed both with and without the Brindley correction to check the influence of the lower absorption coefficient of Si (63.94 cm<sup>2</sup>/g) than that of HfO<sub>2</sub> (133.48 cm<sup>2</sup>/g). Because together with the larger particle size of Si, this may result in overestimation of Si content in the quantitative phase analysis. As Si particle size in the powder varies between 1 to 20 µm (see Fig.1a, d), these two sizes were separately considered in the Brindley correction. The results with the Brindley correction using 1 µm as Si particle size and the results without the correction gave the same Si content of 34 wt. %±3 wt. %, which was in good agreement with the chemical analysis (ICP-OES) results of the powder (33 wt. % ±0.12 wt. %). However, using the larger Si particle size in the Brindley method yielded significantly less Si phase fraction (~ 20 wt%). Therefore it was eventually chosen to apply no corrections on the quantitative analysis of the feedstock and the as-sprayed coating and these results are also shown in Fig.2. After plasma spraying of the powder, in addition to HfO<sub>2</sub> (t) and (m), HfO<sub>2</sub> – cubic (c) (ICSD 53033) and intermetallic HfSi<sub>2</sub> phase (orthorhombic, ICSD 16697) were detected in the deposited coating. The XRD patterns of Si powder and as-sprayed Si coating are not shown here but both were indexed solely with a cubic phase (ICSD 51688).

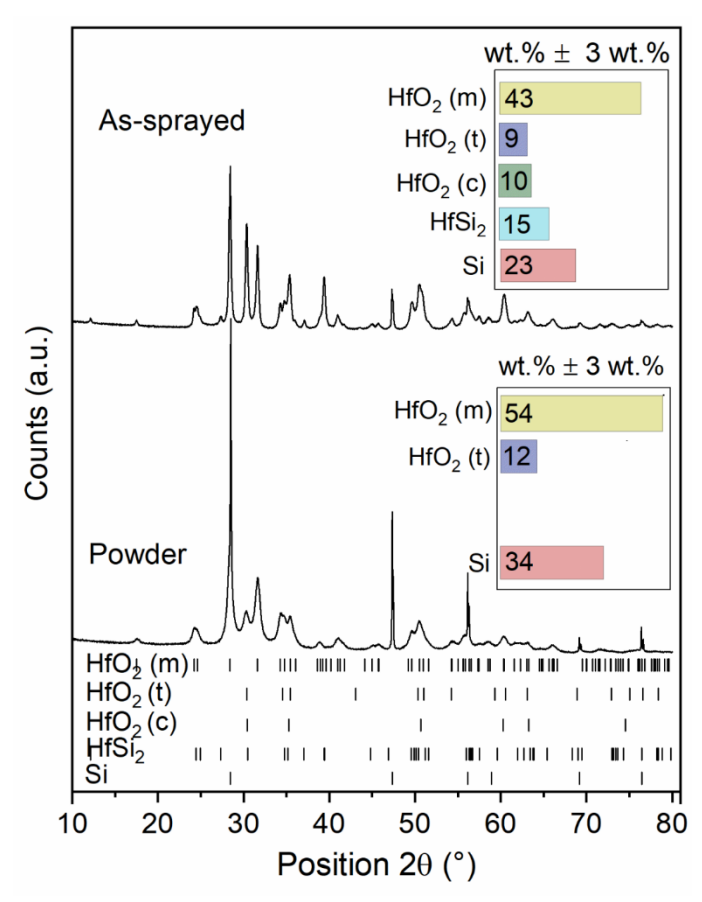


**Figure 2**: XRD patterns of Si-HfO<sub>2</sub> feedstock and as-sprayed coating. Quantitative phase analysis results are shown in the inserted bar charts.

After the APS deposition of Si-HfO $_2$  powder, no significant compositional difference was detected, i.e. the Si concentration in the powder and the coating was 34  $\pm$  3 wt.% and 26.5  $\pm$  3 wt.%, respectively. The low power-high velocity spray conditions adapted for the deposition could be the reason for minimal Si evaporation. Additionally, the powder morphology could be another factor affecting the degree of evaporation. It is known from the previous studies with different chemical powder compositions that, evaporation during plasma spraying excessively takes place at particle surfaces due to overheating. As the Si particles are embedded within the spherical hafnia particles in this work, the temperature gradient in the porous particles could have a diminishing effect on evaporation. On the other hand, as shown in Figure 1, the size of Si particles within the spherical hafnia particles are rather small (roughly in the range of 1-10  $\mu$ m) which implies a higher surface area for evaporation.

The pure hafnia is monoclinic at room temperature and transforms to a tetragonal phase above 1650 °C, while tetragonal to cubic transformation takes place at even higher temperatures (>2500 °C) [18, 19]. The presence of tetragonal and cubic hafnia phases in the as-sprayed coating can be associated with plasma spray deposition wherein powder particles melt in the hot plasma and then rapidly solidify on the substrate (cooling rates > 10<sup>5</sup> K/s). Under these conditions, the thermodynamic equilibrium state might not have reached.

To investigate the stability of high temperature (t) and (c) hafnia phases observed in the feedstock and the coating at room temperature, a HT-XRD investigation was conducted. Fig. 3a shows the recorded patterns of the as-sprayed HfO<sub>2</sub>-Si coating between RT and 1200 °C. Results show that the largest hafnia tetragonal/cubic phase peak (2θ=30.3°) and HfSi<sub>2</sub> peaks (2θ=27.3° & 37°) disappear above 700 °C. The corresponding Rietveld results for quantification are shown in Fig. 3b. While weight percentages of HfO<sub>2</sub> (t) and (c) as well as HfSi<sub>2</sub> approach zero above 700 °C, that of HfO<sub>2</sub> (m) makes a jump from 50 to 65 wt.% at 700 °C and further increases with the increasing temperature. These suggest that HfO2 (t) and (c) are metastable phases and HfO<sub>2</sub> (t) and (c) transform into monoclinic polymorph. At 500-600 °C, a reduction in the wt. % of the HfO2 (c) phase is visible while wt. % of HfO2 (t) increases concurrently. This could imply that the cubic phase first transforms into the tetragonal phase in this lower temperature region and then tetragonal transforms to monoclinic above 600 °C. Very few reports on metastable HfO<sub>2</sub> (c) are available in the literature due to the high melting point of HfO<sub>2</sub> and ultrafast quenching required to retain cubic form at room temperature. Zirconia with similar characteristics to HfO<sub>2</sub> is a more widely investigated material and the presence of metastable cubic and tetragonal zirconia was reported in the plasma sprayed and magnetron sputtered coatings [20-23]. Temperature-dependent transformation of these metastable phases however was not always elucidated, mostly evidence was shown that the metastable phase had transformed after high-temperature annealing. Among these, Ji et al. reported that metastable tetragonal zirconia starts to transform into the monoclinic phase at 500 °C [21]. Synthesis of

metastable cubic and tetragonal zirconia was also reported via the sol-gel route. In this case, several studies showed the same phase transformation path  $(c \rightarrow t \rightarrow m)$  [24, 25] observed in this work however transformation temperatures largely differed (400-800°C) depending on the zirconia crystallite size and pH level of precipitation [26].

As shown in Fig.3b, the amount of HfSi<sub>2</sub> reduces above 600 °C, which could be associated with oxidation. Tsunoura et al. tested oxidation of HfSi<sub>2</sub> above 800°C and reported that it takes oxygen and transforms into HfO<sub>2</sub> and Si (HfSi<sub>2</sub> +  $O_2 \rightarrow$  HfO<sub>2</sub> + 2Si) [27]. Accordingly, an increase for Si can be anticipated above this temperature range. However, on the contrary, a gradual reduction in the weight percentage of Si can be observed in Fig. 3b above 800 °C and this is presumably due to oxidation of Si. Oxidation product SiO<sub>2</sub> is expected to be very thin and amorphous up to 1200°C. When room temperature XRD patterns of the sample before and after HT-XRD measurements were compared, a small background rise was detected between 20=18-23° (see supplementary material) which might be associated with the amorphous SiO<sub>2</sub>. The formation and oxidation of HfSi<sub>2</sub> will be further discussed below together with microstructural observations.

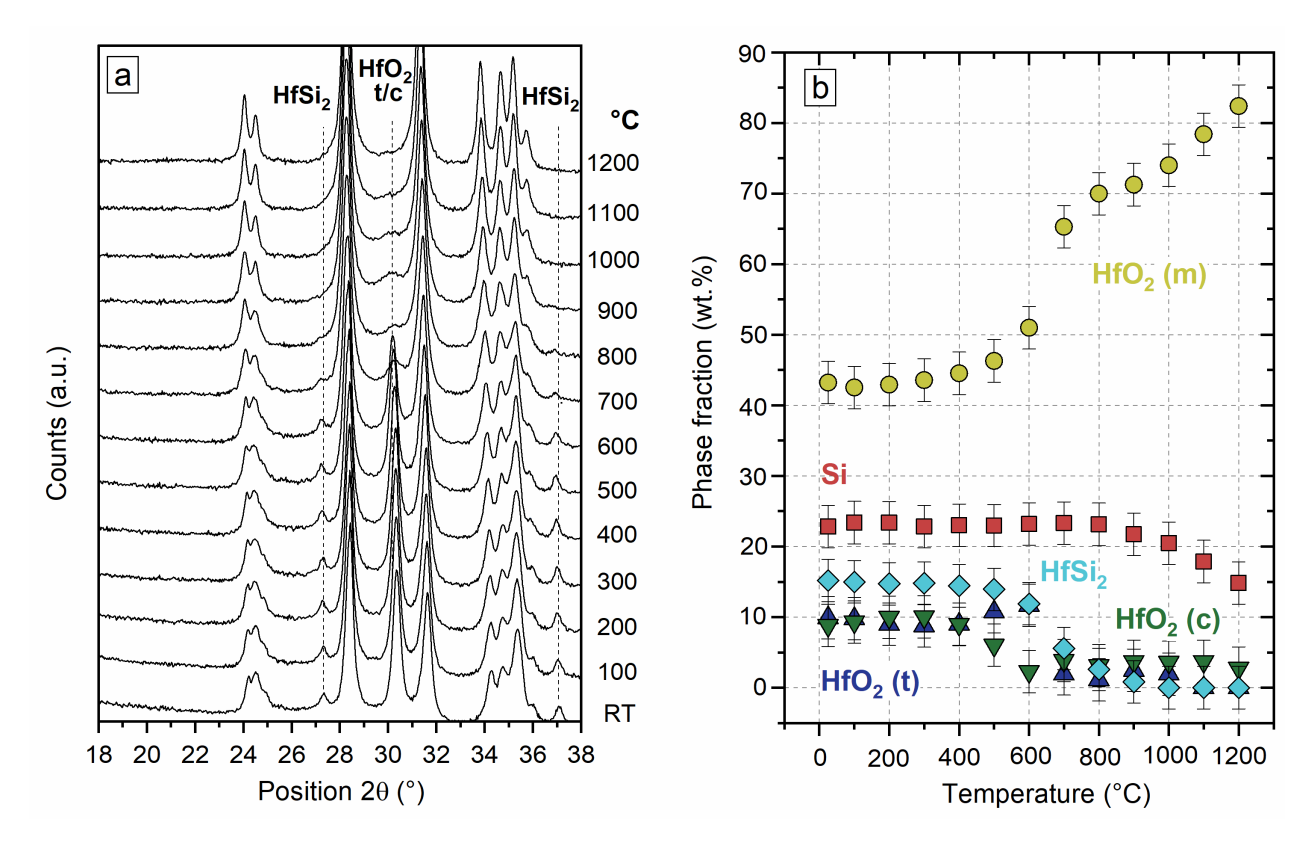


**Figure 3:** The HT-XRD patterns of the as-sprayed Si-HfO $_2$  coating between RT and 1200 °C (a), quantitative phase analysis results of the XRD data (b).

# 3.2. The microstructure of the as-sprayed coating

In Fig. 4 (a-e), BSE-SEM images show the cross-section microstructure of as-sprayed Si-HfO<sub>2</sub> bond coat wherein different phases are distinguishable. According to EDS analysis results (1-6), shown in Fig. 4f-h, the dark gray phase is silicon (EDS spectrum 1-2), the brightest phase is hafnia (EDS spectrum 5-6) and the medium gray phase (EDS Spectrum 3-4), which shows a very fine lamellar type of structure, is hafnium and silicon-rich. These results are in good agreement with the XRD analysis results of the as-sprayed coating, where the main phases were found to be HfO<sub>2</sub>, HfSi<sub>2</sub>, and Si. In the as-sprayed coating microstructure, additionally, dendritic type of structures with fine branches was observed in the Si-rich regions (visible in Fig.4b and e) implying non-equilibrium solidification conditions. The composition of these however could not be resolved via EDS.

Based on the compositional information and microstructural features, it can be concluded that Si particles were completely melted in the thermal spray process while hafnia particles could be only partially melted (Fig. 4e). This can be well explained by the approximately two times higher melting point of HfO<sub>2</sub> (2810°C [18]) than that of Si (1414 °C). Due to the low melting point, Si particles that are contained in the HfO<sub>2</sub> agglomerates likely melt first, this results in the breaking of the agglomerate and finally dispersion of the submicron hafnia particles within the molten Si matrix (Fig. 4b-c). In some regions, primary hafnia particles in the Si matrix are separated from each other indicating that they were only loosely bonded. It can be easily seen from Fig. 4 that, the Hf and Si-rich phase (HfSi<sub>2</sub> according to XRD analysis results) with medium gray contrast forms near the dispersed submicron hafnia particles in the Si-matrix.

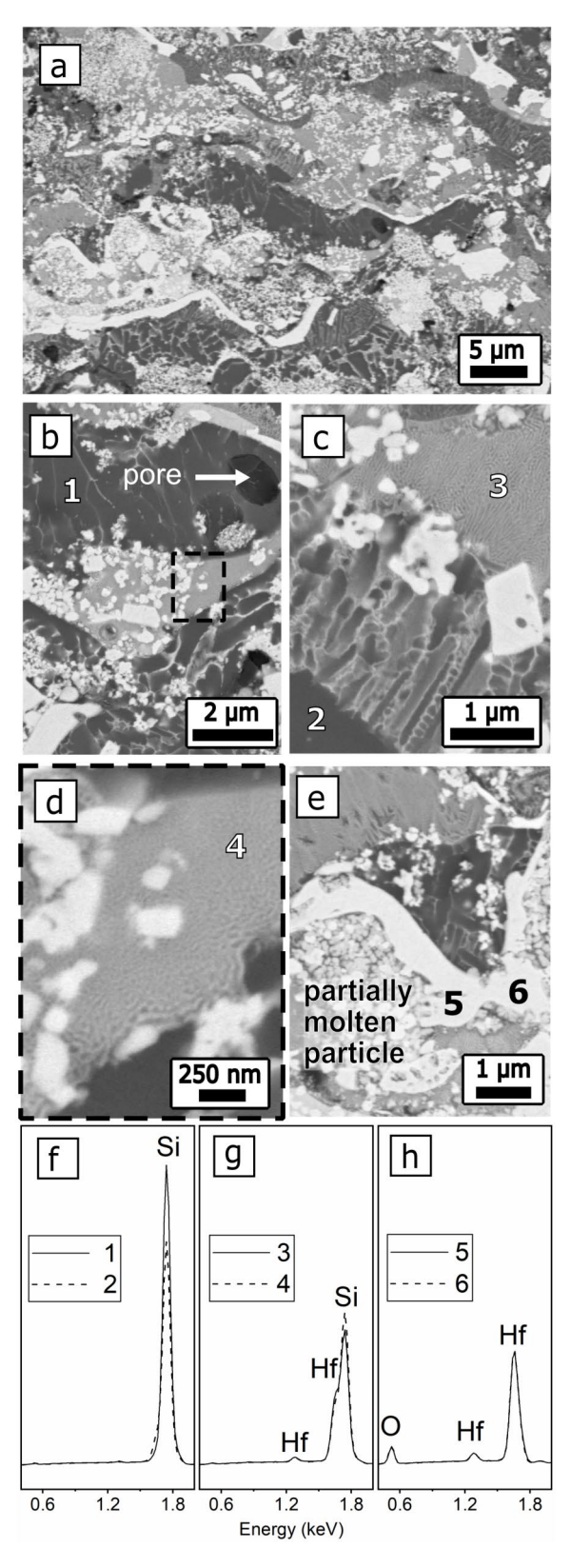


**Figure 4**: Cross-section SEM images of atmospheric plasma-sprayed bond coat from Si-HfO<sub>2</sub> powder (a—e), and EDS spectra of points (1—6) (f, g, h) shown in (b—e). Image (d) is the higher magnification image of the rectangular field marked with a dashed line in (b).

# 3.3. HfSi<sub>2</sub> formation in the plasma spray process

Both XRD analysis results and microstructural characterizations suggest the presence of the HfSi<sub>2</sub> phase in the as-sprayed coating however, the formation mechanism of HfSi<sub>2</sub> is not fully understood. Thermodynamic stability analyses suggest that HfO<sub>2</sub>-Si interfaces are stable up to 1600 K [28-30]. However, these analyses only consider the reactions between the two stoichiometric solids, which does not represent the experimental conditions in this work.

In the literature,  $HfSi_2$  formation at the interface of an  $HfO_2$  coating and Si substrate via solid-state reaction was reported upon vacuum annealing (700-1000 °C) [31-33]. The driving force for the formation of  $HfSi_2$  was linked to oxygen deficiency in the  $HfO_2$  deposit, which may result from a non-equilibrium deposition process or reducing atmosphere in the deposition process or low oxygen partial pressure ( $P_{O2}$ ) during high-temperature treatment [34]. It was proposed that if oxygen is not available in the atmosphere, the free energy of the oxygen-deficient metal oxide ( $MO_{2-x}$ , stands for  $HfO_2$  here) and Si system can be lowered by the reaction of excess M with Si, leaving behind a stoichiometric oxide [35]:

$$MO_{2-x} + xSi \rightarrow (1 - x/2)MO_2 + x/2MSi_2$$
 (1)

In this work, neither a reducing atmosphere nor low P<sub>O2</sub> was employed in the atmospheric plasma spraying process. Yet, from the existence of the metastable phases in the as-received feedstock (HfO<sub>2</sub> (t)) and the as-sprayed coating (HfO<sub>2</sub> (t), (c)), it is evident that both powder and the coating were not in thermodynamic equilibrium. It is widely agreed in the literature that stabilization of tetragonal and cubic phases at room temperature is due to the presence of oxygen vacancies and resultant lattice distortion in nano ZrO<sub>2</sub> and HfO<sub>2</sub> particles and thin films [36-38]. Therefore, it is not unrealistic to assume oxygen deficiency in the submicron hafnia particles of the feedstock and the as-sprayed coating. As submicron hafnia particles were dispersed in the molten silicon before solidification, wherein oxygen was not readily available at the particle-Si interface, a similar mechanism described above according to the reaction (1)

might be responsible for the formation of HfSi<sub>2</sub> in the plasma spray process. Assuming that the reaction (1) is HfO<sub>2</sub> limited, by solving it according to 15 wt.% HfSi<sub>2</sub> (~5 mol. %) detected in the as-sprayed coating via XRD, the oxygen sub-stoichiometry (2-x) in the hafnia can be estimated as 1.9. There is unfortunately no reported study on the oxygen deficiency levels of plasma-sprayed hafnia or zirconia for comparison. In an early work, oxygen sub-stoichiometry in atmospheric plasma sprayed yttria-stabilized zirconia (8 wt.% Y<sub>2</sub>O<sub>3</sub>-ZrO<sub>2</sub>) was reported as 1.94 [39]. This value is not far off from the estimation made here, however it is well expected that the chemical composition and manufacturing route of the starting powder, as well as plasma spray conditions (e.g. plasma power, plasma gas composition), can strongly affect the oxygen sub-stoichiometry of the deposited coating. Therefore further investigation is required to understand whether or not oxygen vacancy has a role in the HfSi<sub>2</sub> formation mechanism.

# 3.4. Thermal expansion behavior via Dilatometry and HT-XRD

The dilatometry measurement results of the as-sprayed Si and Si-HfO<sub>2</sub> coatings are shown in Fig. 5. A rather linear thermal expansion during heating was observed for the Si coating between RT and 1200 °C. The calculated linear coefficient of thermal expansion (CTE) of the Si coating was  $4.58 \times 10^{-6} \, \text{K}^{-1}$  in the given temperature range. The Si-HfO<sub>2</sub> coating, on the other hand, showed a non-linear expansion during the heating period, i.e. the length of the sample (#1) increased rapidly up to ~750 °C, and above this temperature, it continued to expand linearly. A large part of the non-linear expansion took place between ~600-750 °C. During cooling down, the sample yielded a linear contraction but did not reach the original length at room temperature implying that an irreversible change occurred in the heating period. It should be mentioned that measurement was repeated with a second sample and the results were reproducible.

XRD analysis after the dilatometry measurement revealed no metastable phases in the coating as shown in Fig. 6a. Supporting this finding, no indication of HfSi<sub>2</sub> phase, which was evident around the primary hafnia particles in the as-sprayed microstructure as shown in Fig. 4, was

observed in the microstructure after the dilatometry measurement (Fig. 6b, c). Furthermore non-linear expansion behavior of the coating up to ~750 °C coincided well with the high-temperature XRD analysis results of the as-sprayed Si-HfO<sub>2</sub> coating, which showed that the metastable phases disappear above 700 °C (Fig. 3b). To measure the CTE of the coating without metastable phases a stabilization heat treatment (1200 °C-5 h-air-10 K/min heating and cooling rate) was applied to an as-sprayed Si-HfO<sub>2</sub> sample prior to dilatometry measurement. After this short heat treatment, which was deliberately kept short to minimize the oxidation and hence its influence on the expansion behavior, the absence of metastable phases was confirmed by XRD and SEM analysis (Fig. 6 a, d, e). Nevertheless it should be noted a small silica peak (α-cristobalite) was visible at 20≈22-23° after the heat treatment which may have slightly affected the measured CTE shown in Fig. 5. It can be seen that the heat-treated sample yielded a linear expansion during the heating period up to 1200 °C contrary to as-sprayed Si-HfO<sub>2</sub> coating. The linear CTE of the heat-treated Si-HfO<sub>2</sub> coating between RT and 1200 °C was 4.8 x10-6 K-1, which is close to that of the Si coating as well as monolithic SiC (4.77x10-6 K-1).

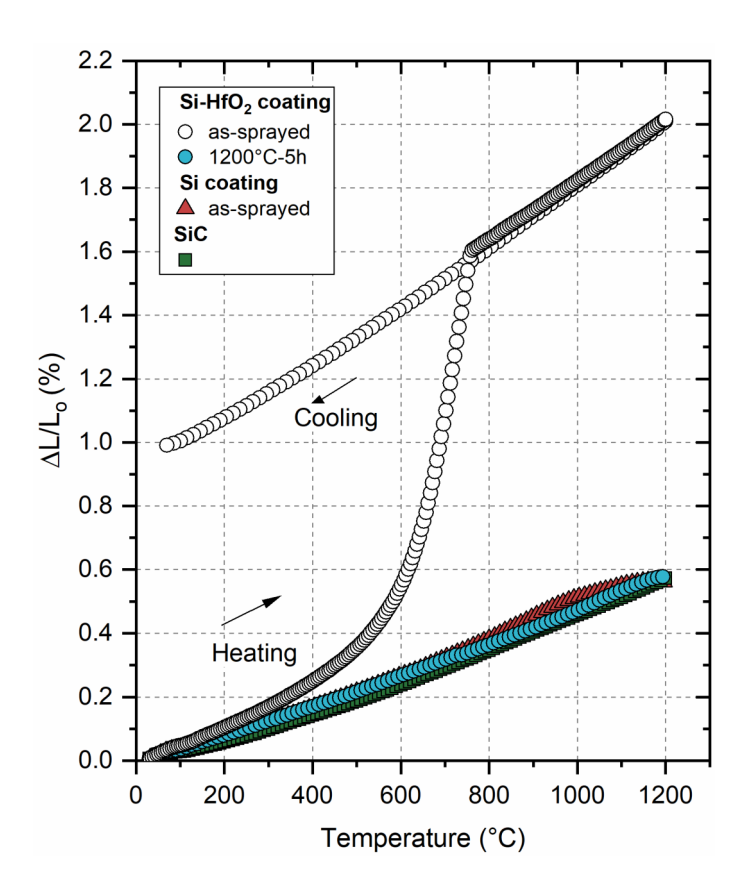


**Figure 5**: Dilatometry measurements results of freestanding Si and Si-HfO<sub>2</sub> as-sprayed coatings, heat-treated (1200 °C-5 h) Si-HfO<sub>2</sub> coating as well as SiC in air.

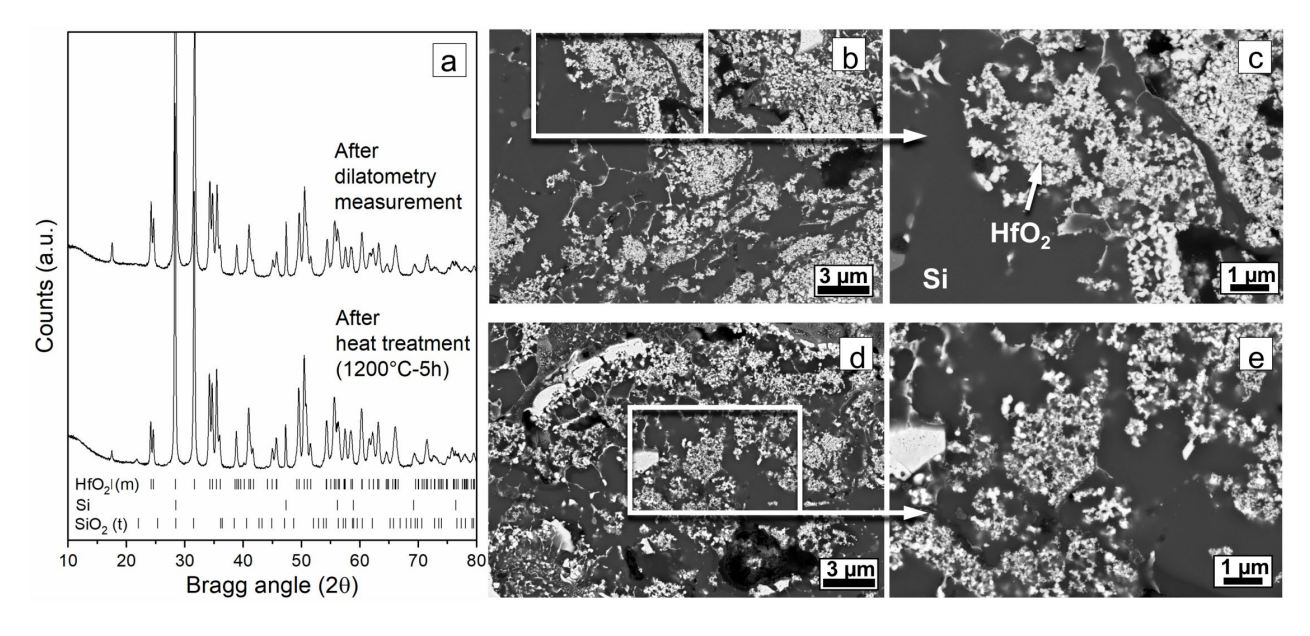


**Figure 6**: XRD patterns of Si-HfO<sub>2</sub> coating after dilatometry measurement and heat treatment  $(1200^{\circ}\text{C-5h}, \text{ air})$  (a), microstructure of the coating after dilatometry measurement (b, c) and heat treatment (d, e).

Based on these experimental results, the non-linear expansion of the as-sprayed Si-HfO2 coating up to ~750 °C was associated with the presence of HfO<sub>2</sub> (t), HfO<sub>2</sub> (c), and HfSi<sub>2</sub>. The volume change of the coating was estimated to be ~3.6% ( $\Delta V/V_0 \cong 3\Delta L/L_0$ ) at ~750°C. This was done by subtracting the length change  $(\Delta L/L_0)$  of the heat-treated sample from that of the as-sprayed sample at the given temperature and with the assumption that heat-treated (1200°C-5h) sample displayed solely the thermal expansion of the coating due to the absence of metastable phases. Following that, the volume expansions in polymorphic transitions of HfO2 and oxidation of HfSi<sub>2</sub> were estimated using HT-XRD data and compared to the dilatometry measurement result. Temperature-dependent normalized unit cell volumes ( $V_{cell}/z$ , z=number of formulas in the unit cell, i.e. z= 4 for HfO<sub>2</sub> (m), z= 2 for HfO<sub>2</sub> (t), z= 4 for HfO<sub>2</sub> (c), z=4 for HfSi<sub>2</sub> and z=8 for Si) were calculated for each phase and Fig. 7 shows the  $V_{cell}/z$  values for the three HfO<sub>2</sub> polymorphs. The data points could be best described by polynomial functions for HfO<sub>2</sub> (c) and (t) indicating that the dependence of the lattice volume on temperature is not linear for these phases. According to the HT-XRD quantitative phase analyses results shown in Fig. 3b, HfO<sub>2</sub> (c) and (t) coexist up to 400 °C, HfO<sub>2</sub> (c)  $\rightarrow$  (t) transformation takes place at ~500-600°C, while HfO<sub>2</sub> (t)  $\rightarrow$  (m) transformation occurs at 600-700°C. Based on that, volume change accompanied by the (c) $\rightarrow$ (t) transformation at 500 °C and (t) $\rightarrow$ (m) transformation at 700 °C was calculated as +0.7% and +3.7%, respectively. As a first approximation, the volume change in the coating associated with these phase transformations can be taken as proportional to the volume fractions of the phases. Volume fractions of the phases were estimated as follows, molar mass (M) and molar volumes ( $V_m = N_A V_{cell}/z$ ,  $N_A$  is Avogadro constant) of the compositions were used to determine the densities of the phases  $(\rho(T)(g/cm^3) = M(g/mol)/V_m(T)(cm^3/mol))$ and densities were used to convert weight fractions of the phases to the volumetric fractions. Accordingly volume fractions of both HfO<sub>2</sub> (c) and HfO<sub>2</sub> (t) were ~0.05 at 400°C (as the reaction takes place at 500°C, the closest volume fraction to that was taken for the estimation) and the volume fraction of the tetragonal phase at 600 °C was ~0.1. Consequently, volume expansion of

the coating due to  $HfO_2$  phase transformations can be estimated as ~0.035% at 500°C and 0.37% at 700°C, a total of ~ 0.4%, which is too small to explain ~3.6 vol. % expansion observed in dilatometry measurement as described above.

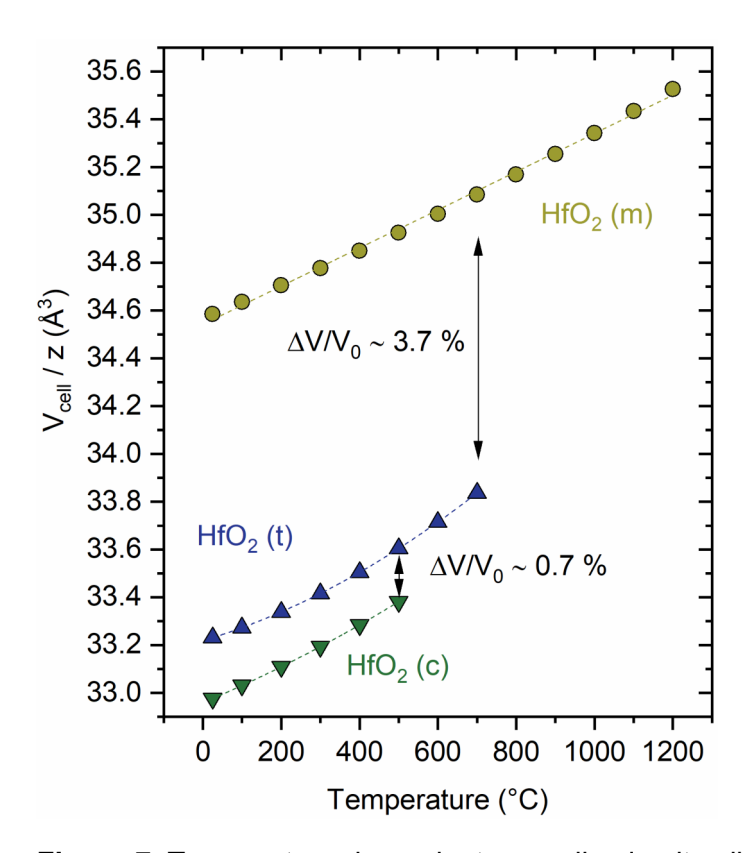


**Figure 7**: Temperature-dependent normalized unit cell volumes for  $HfO_2$  (c),  $HfO_2$  (t), and  $HfO_2$  (m) phases. Dashed lines are the polynomial (for  $HfO_2$  (c) and (t)) and linear (for  $HfO_2$  (m) fitted lines to the data points. Error bars are smaller than the symbols.

Secondly, the volume change involved in the oxidation reaction of  $HfSi_2$  ( $HfSi_2+O_2\rightarrow HfO_2+2Si$ ) was estimated from the HT-XRD data. From the effective volume change calculated for this reaction ( $\Delta V^{eff} = (V_m^{HfO2} + 2V_m^{Si})/V_m^{HfSi2}$ ), using the molar volume of the phases at 700 °C ( $V_m^{HfO2} = 21,132 \, cm^3/mol, V_m^{Si} = 12,146 \, cm^3/mol, V_m^{HfSi2} = 29,936 \, cm^3/mol$ ), the volume expansion was estimated to be 51%. The volume fraction of the  $HfSi_2$  phase was determined as 0.084, which yields ~4.2% volume expansion in the coating at 700 °C. This expansion alone was already greater than the anticipated volume expansion based on the dilatometry measurement. The error could be attributed to differences in the transformation and oxidation kinetics between dilatometry and HT-XRD (due to different heating rates and dwell times in HT-XRD), CTE

difference between the as-sprayed and heat-treated coating due to metastable phases in the former (different CTE between the constituents could induce thermal stresses) and oxidation in the latter as well as porosity in the coating which could reduce expansion in dilatometry measurement upon oxidation. After all, according to these estimations, the large expansion of the coating around 700°C is expected to be due to the oxidation of HfSi<sub>2</sub> rather than the polymorphic transitions of the hafnia. It should be also noted that Si oxidation-induced volume increase was omitted in the calculations here as there was no detectable change in Si content of the coating up to 800 °C in HT-XRD measurements (Fig.3b).

# 3.5. Phase composition and microstructure – after thermal cycling

Fig.8 shows the XRD analysis results taken from the Si-HfO<sub>2</sub> coating surface after 1<sup>st</sup> (10 h), 2<sup>nd</sup> (20 h), 3<sup>rd</sup> (30 h), 5<sup>th</sup> (50 h), and 10<sup>th</sup> (100 h) cycle at 1300 °C. After 10 h exposure at 1300 °C, SiO<sub>2</sub> ( $\alpha$ -cristobalite) and HfSiO<sub>4</sub>, (hafnon) peaks became visible. The former is the oxidation product of silicon while the latter forms via the reaction of SiO<sub>2</sub> and HfO<sub>2</sub> (SiO<sub>2</sub>+HfO<sub>2</sub> $\rightarrow$ HfSiO<sub>4</sub>). As shown in the graph the Si peak at 20=47° (marked with the arrows) disappeared after the 50 h but as will be discussed below, even after 100 h exposure, micrographs revealed small silicon islands within the oxidized SiO<sub>2</sub> regions. This can be attributed to a different rate of oxidation at the surface of the coatings, which was analyzed by XRD in this work, and at the internal portion of the coatings which was only observed by the SEM. After each cycle, the intensity of HfO<sub>2</sub> peaks reduced, SiO<sub>2</sub> peaks remained similar (ongoing Si oxidation and reaction with HfO<sub>2</sub>) and that of HfSiO<sub>4</sub> peaks increased.

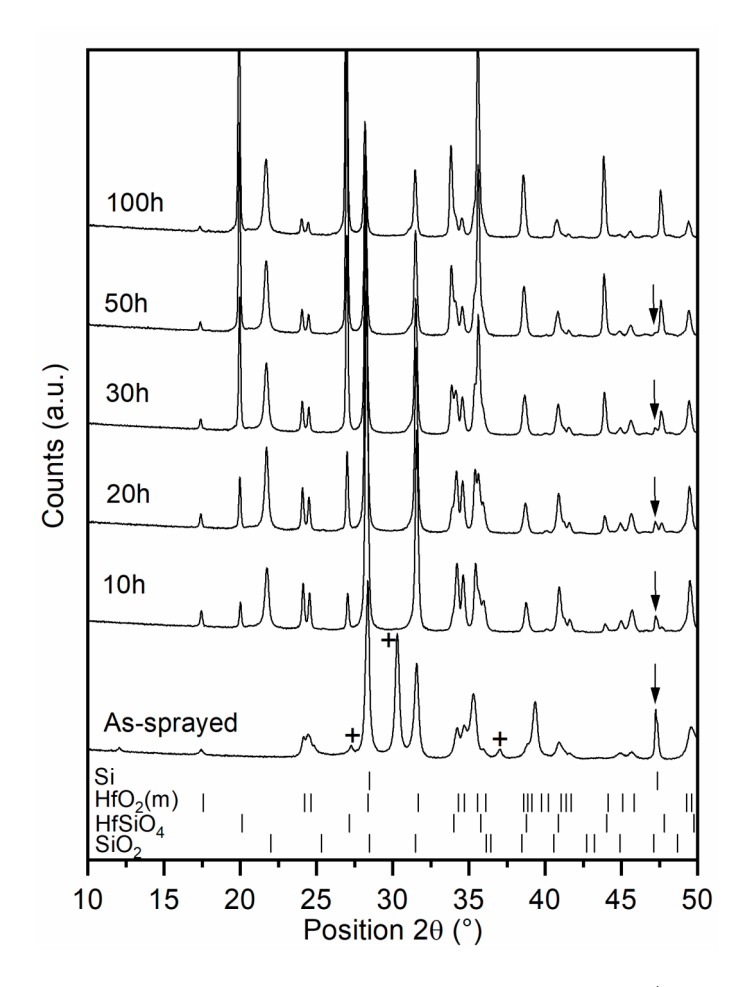


**Figure 8**: Phase composition of Si-HfO<sub>2</sub> after 1<sup>st</sup> (10 h), 2<sup>nd</sup> (20 h), 3<sup>rd</sup> (30 h), 5<sup>th</sup> (50 h), and 10<sup>th</sup> (100 h) cycle at 1300 °C in air. The plus sign (+) indicates the metastable phases in the assprayed coating and the arrows were used to mark the Si peak at  $2\theta$ =47°.

A comparison of quantitative phase analysis results after 10 h and 100 h is shown in Table 2.

The results are given both with and without the Brindley correction to demonstrate the influence of the lower absorption coefficient of  $SiO_2$  (36.01 cm²/g) and Si (63.94 cm²/g) in comparison with that of other constituents (HfO2:133.48 and HfSiO4:111.84 cm²/g). For the Brindley correction particle sizes of Si and  $SiO_2$  were chosen based on the micrographs of the coatings after 10 h and 100 h thermal cycling (Fig. 9). The Si and  $SiO_2$  particle sizes were taken as 15  $\mu$ m and 1  $\mu$ m, respectively for the correction after 10 h thermal cycling. As there was no Si peak at the XRD pattern after 100 h thermal cycling, assuming that Si particles were completely transformed into  $SiO_2$ , the correction was only made using 15  $\mu$ m as  $SiO_2$  particle size. Consequently, phase fractions with or without correction were found to be quite similar after 10 h thermal cycling

considering the margin of error of the analysis (±3 wt. %). After 100 h thermal cycling, however, the estimated SiO<sub>2</sub> content without the correction was significantly large in comparison with the corrected analysis results. This suggested that when the low absorption coefficient of SiO<sub>2</sub> is combined with large SiO<sub>2</sub> particle sizes, it may lead to an overestimation of SiO<sub>2</sub> content and that makes the correction necessary.

Table 2: Quantitative phase analysis results of the XRD data ex-situ measured during thermal cycling.

Time at 1300 °C	Si (wt.% ±3 wt.%)	SiO <sub>2</sub> (wt.% ±3 wt.%)	HfO <sub>2</sub> (m) (wt.% ±3 wt.%)	HfSiO <sub>4</sub> (wt.% ±3 wt.%)
10 h (without correction)	7	22	64	7
10 h (with Brindley correction)	4	21	68	7
100 h (without correction)	-	25	17	58
100 h (with Brindley correction)	-	14	20	66

Cross-section SEM images of the thermally cycled Si-HfO $_2$  coating (1300 °C-air) after the first cycle (10 h) and the tenth cycle (100 h) are shown in Fig. 9a-d. After the first thermal cycle, the coating was vertically cracked (Fig. 9a) and a thin SiO $_2$  layer (<1  $\mu$ m) was visible around the large Si particles (10-15  $\mu$ m) within the microstructure (Fig.9b). It can be also seen in Fig. 9a that under the vertical cracks the coating was partially delaminated from the substrate. After the tenth cycle (Fig. 9c-d), the vertical crack openings were larger and the coating was also horizontally cracked. Under the vertical cracks, thermally grown silica thickness at the surface of SiC/SiC CMC was 2.74  $\pm$  0.5  $\mu$ m while in the regions without vertical cracks, where the coating was still attached to the substrate, it was 1.2  $\pm$  0.1  $\mu$ m (Fig.9a). The latter is comparable with the oxide thickness (1.38  $\pm$  0.2) reported after 100 h air exposure at 1371 °C, for a SiC substrate coated with ~50  $\mu$ m Si-HfO $_2$  bond coat and ~150  $\mu$ m EBC [13].

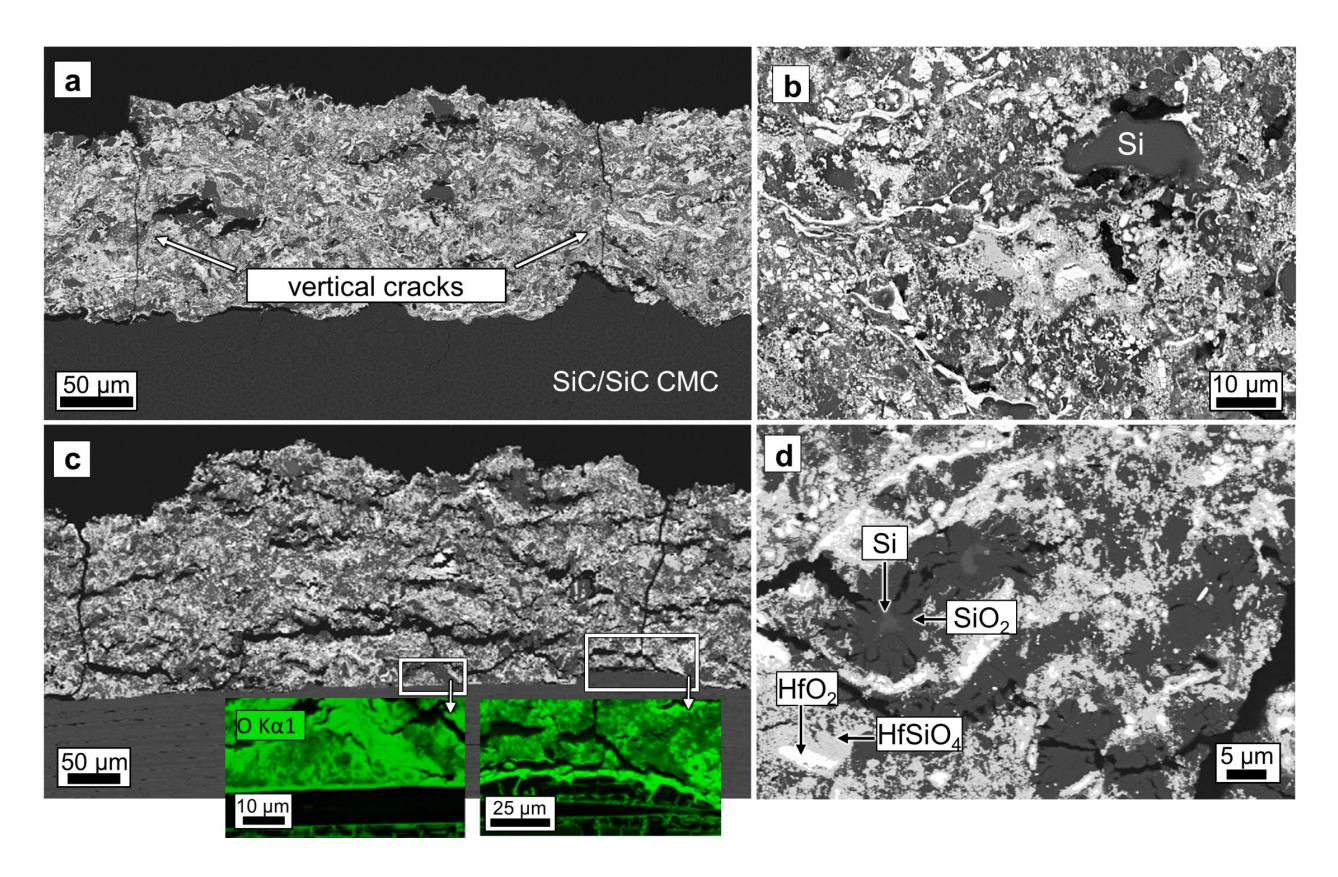


**Figure 9**: Cross-section SEM microstructure of thermally cycled (1300°C-air) Si-HfO2 coating on SiC/SiC CMC after 10 h (a, b) and 100 h (c, d). Oxygen EDS maps belong to the framed areas in (c).

Observed vertical cracking in the coating after the first thermal cycle could be attributed to the non-linear expansion of the coating within the first heating cycle (up to  $\sim$ 750°C) as found in the dilatometry measurements (Fig.5). This expansion could have led to compressive stresses in the constrained coating by the substrate and relaxed by cracking and delamination. Extensive cracking after the tenth cycle also indicates high-stress levels in the coating during thermal cycling. Oxidation induced stresses due to large volume expansion upon oxidation of Si (117% based on the molar volumes Si and SiO<sub>2</sub> measured in this work) and reversible  $\beta$ - $\alpha$  cristobalite transition that is accompanied also by volume change ( $\sim$ 5%) could be accounted for this. Microcracking in the SiO<sub>2</sub> scale around a Si core shown in Fig. 9d is a possible consequence of these phenomena. The contribution of SiO<sub>2</sub> phase transitions to the macro cracking in the coating also cannot be ruled out because SiO<sub>2</sub> has a significant volume fraction in the coating

after thermal cycling. According to Rietveld analysis results with the Brindley correction, after 100 h thermal cycling, volume fractions of SiO<sub>2</sub>, HfO<sub>2</sub> and HfSiO<sub>4</sub> in the coating are 0.34, 0.10, and 0.56, respectively, at room temperature. Related to that, the ideal would be large consumption of SiO<sub>2</sub> to form the hafnon phase, which is a stable phase, has close CTE (3.11-5.97x10<sup>-6</sup> K<sup>-1</sup> at 100-1250°C [14]) to the rest of the system and additionally hafnon formation reduces the molar volume by ~18% ( $V_m^{HfSiO4}=38.822$ ,  $V_m^{HfO2}=20.830$ ,  $V_m^{SiO2}=$  $26.281 \ cm^3/mol$ ) at RT. Deijkers and Wadley recently made oxidation experiments on a model system where Si particles (25 µm) were immersed in the HfO<sub>2</sub> matrix [40]. They compared the net rate of SiO<sub>2</sub> formation on Si particles with and without HfO<sub>2</sub> present. The results revealed that the thickness of the SiO<sub>2</sub> layer during high-temperature oxidation (1250°C-1316°C) can be greatly reduced by the hafnon formation reaction in the presence of the hafnia matrix. This suggests that if the coating microstructure and chemical composition can be optimized, HfO2 addition in Si is a viable approach to reduce the thickness of the detrimental SiO<sub>2</sub> layer. In our work, however, the large volume fraction of SiO<sub>2</sub> after 100 h thermal cycling implies that hafnon formation was possibly hindered by a low volume fraction of HfO<sub>2</sub>, inhomogeneous dispersion of HfO<sub>2</sub> in Si (see Fig.9b-d), and cracks/pores which exacerbate the poor contact between SiO<sub>2</sub> and HfO<sub>2</sub> phases.

The contribution of CTE mismatch stresses to the cracking should be also considered. Table 3 summarizes the CTE values of the phases that exist in the coating during thermal cycling. Using these and room temperature volume fractions of the phases after stabilization treatment (1200°C-5 h, Si: 0.45, HfO<sub>2</sub>=0.55) and after thermal cycling (1300°C, 100 h, SiO<sub>2</sub>:0.34, HfO<sub>2</sub>: 0.10, HfSiO<sub>4</sub>:0.56), CTE of the coating was estimated at 100°C and 1200°C. For the high-temperature calculation, volume fractions of the phases were assumed the same with room temperature. Accordingly, the CTE of the coating after stabilization treatment was found to be 5.07x10<sup>-6</sup> K<sup>-1</sup> at 100°C and 5.91x10<sup>-6</sup> K<sup>-1</sup> at 1200°C. These values reasonably agree with the linear CTE of the

coating measured by dilatometry (4.8 x10<sup>-6</sup> K<sup>-1</sup>, RT-1200°C, Fig.5). After thermal cycling, the CTE was  $5.89 \times 10^{-6}$  K<sup>-1</sup> at  $100^{\circ}$ C and  $5.17 \times 10^{-6}$  K<sup>-1</sup> at  $1200^{\circ}$ C. The reason that CTE reduces at high temperature is the lower CTE of  $\beta$ -cristobalite than that of  $\alpha$ -cristobalite. Nonetheless, the CTE of the coating varies between  $5-6 \times 10^{-6}$  K<sup>-1</sup> due to compositional change upon oxidation and as a function of temperature. This change is not substantial and the CTE of the coating is not significantly different from that of the substrate (4.77 x10<sup>-6</sup> K<sup>-1</sup> at RT-1200°C, according to dilatometry measurement). Therefore, only a minor contribution, if any, of CTE mismatch stresses to the cracking of the coating is anticipated. Lastly, it should be noted that CTE differences between Si and HfO<sub>2</sub> could lead to stress build-up in the coating at the initial stages of thermal cycling. At the test temperature, Si is expected to creep substantially and allow HfO<sub>2</sub> to freely expand. Upon cooling, Si will be under tensile stresses due to the larger CTE of HfO<sub>2</sub> which could be an additional driving force for cracking in the coating.

Table 3: Thermal expansion coefficient (CTE) of the phases in the coating.

Phase	CTE (10 <sup>-6</sup> K <sup>-1</sup> )	Temperature (°C)	Ref.
Si	3.37-3.70	100-1200	This work*
HfO <sub>2</sub> (m)	6.46-7.72	100-1200	This work*
HfSiO <sub>4</sub>	3.11-5.97	100-1250	[14]
α-cristobalite	10.3	Not defined	[15]
β-cristobalite	3.1**	Not defined	[15]

<sup>\*</sup> The linear isotropic thermal expansion coefficient  $(\alpha_{isotr.})$  was calculated through the volumetric expansion coefficient  $(\beta_v)$  as  $\alpha_{isotr.} \cong \beta_v/3$ .  $\beta_v$  was determined from HT-XRD data according to:

 $\beta_v(T) = (V_{cell}(T) - V_{cell}(298K) / V_{cell}(298K) (T - 298K))$ 

\*\*According to some other literature, β-cristobalite has zero or negative CTE [41, 42].

It should also be mentioned that no metastable phase or cracking issues in the coatings were reported in the previous studies using the same material system [13, 15]. The main differences e.g. composition, deposition method, and test temperature between this work and earlier studies

are summarized in Table 4. Albeit both PS-PVD and APS are thermal spray processes, high plasma power in the former encourages the melting and vaporization of HfO<sub>2</sub> particles, while as shown in this work partially molten or unmolten HfO<sub>2</sub> particles are deposited in the APS process. Furthermore, the starting powder morphologies were also different in the two processes, the powder consisted of large (~20 μm) Si particles that were 'clad' with smaller (~1–5 μm) HfO<sub>2</sub> particles in [13], which could also significantly impact the HfO<sub>2</sub> state and phase content/distribution in the microstructure. After all, as all mentioned factors influence phase composition, residual stresses, reaction kinetics, etc. in the coatings, it is not possible to explain the performance difference at this time.

Table 4: Comparison of deposition and test conditions in different studies.

	This work	Anton et al.[15]	Harder´s study [13]
Composition (mol. %)	20/80 (HfO <sub>2</sub> /Si)	30-60/70-40 (HfO <sub>2</sub> /Si)	25/75 (HfO <sub>2</sub> /Si)
Deposition method	APS	Magnetron sputtering	PS-PVD
Coating thickness [µm]	150	10	50
Type of microstructure	Dense-splat	Dense-columnar	Dense-splat
Test temperature (°C)	1300	1250	1370-1480

## 4. Conclusions

Si-HfO<sub>2</sub> coatings were deposited using atmospheric plasma spraying from a Si-HfO<sub>2</sub> (80/20 mol. %) feedstock. The coating was characterized in terms of phase composition, and thermal expansion as well as its performance was tested on a SiC/SiC CMC substrate via furnace cycling (1300 °C, 100 h, and 10 cycles). It was found that:

a) The as-sprayed coating contains  $HfO_2$  (m) and Si as well as metastable phases, namely,  $HfO_2$  (t),  $HfO_2$  (c), and intermetallic  $HfSi_2$ . The total volume fraction of these phases was

- 20% in the as-sprayed coating. The powder already had HfO<sub>2</sub> (t), but HfO<sub>2</sub> (c) was observed only after the spray process.
- b) HT-XRD revealed that the metastable phases disappear above 700 °C. HfO₂ (t) and (c) transforms to HfO₂ (m), while HfSi₂ oxidizes above this temperature (HfSi₂+O₂→HfO₂+2Si).
- c) Dilatometry measurements of the as-sprayed Si-HfO<sub>2</sub> coating showed that the coating expands non-linearly up to ~750 °C and a large expansion occurs between 600-750 °C. This behavior was mainly attributed to volume expansion during the oxidation of HfSi<sub>2</sub>.
- d) After the first thermal cycle, the coating was vertically cracked and after the tenth cycle, additional horizontal cracks and extensive oxidation were observed in the coating. As a result, the SiC/SiC substrate was also severely oxidized. The cracking was linked to volume expansion upon oxidation of HfSi<sub>2</sub> as well as oxidation of Si and  $\alpha \leftrightarrow \beta$  phase transitions in cristobalite.
- e) After 100 h at 1300°C, the volume fractions of SiO<sub>2</sub>, HfO<sub>2</sub>, and HfSiO<sub>4</sub> in the coating were 0.34, 0.10, and 0.56, respectively, at room temperature. This result suggests that hafnon formation was likely hindered by insufficient HfO<sub>2</sub> content.

Based on these results, one of the main issues leading to the poor performance of the Si-HfO<sub>2</sub> bond coat under the investigated testing conditions could be identified as the formation of HfSi<sub>2</sub> in the plasma spray process. Because vertical cracking in the coating, which presumably stems from rapid expansion in the first heating cycle due to metastable phases, accelerates the oxidation through the thickness of the coating. HfSi<sub>2</sub> formation is not fully understood but one hypothesis is that oxygen-deficient, submicron HfO<sub>2</sub> particles may be prone to react with molten Si to form the HfSi<sub>2</sub> phase. Further investigations are required to test this hypothesis. Other issues are insufficient hafnia content and inhomogenous distribution of hafnia in Si, which hinders hafnon formation and hence leads to a high volume fraction of detrimental SiO<sub>2</sub> in the

coating. In this regard, further optimizations are required in feedstock composition and morphology.

**Acknowledgments**: The authors are grateful to Prof. Dr. Dietmar Koch for providing SiC/SiC CMC substrates, Marie-Theres Gerhard for dilatometry measurements, Dr. Doris Sebold for SEM-EDS analysis, Frank Kurze for thermal spray assistance, and Mark Kappertz for metallographic sample preparation.

### References

- [1] E. Bakan, D.E. Mack, G. Mauer, R. Vaßen, J. Lamon, N.P. Padture, High-temperature materials for power generation in gas turbines, in: O. Guillon (Ed.), Advanced Ceramics for Energy Conversion and Storage, Elsevier Cambridge, MA,2020, pp. 3-62.
- [2] N.S. Jacobson, Corrosion of Silicon-Based Ceramics in Combustion Environments, J. Am. Ceram. Soc. 76(1) (1993) 3-28.
- [3] E.J. Opila, R.E. Hann, Paralinear Oxidation of CVD SiC in Water Vapor, J. Am. Ceram. Soc. 80(1) (1997) 197-205.
- [4] K.N. Lee, Current status of environmental barrier coatings for Si-Based ceramics, Surf. Coat. Technol. 133–134 (2000) 1-7.
- [5] K.N. Lee, Environmental Barrier Coatings For SiC/SiC, in: N.P. Bansal, J. Lamon (Eds.) Ceramic Matrix Composites: Materials, Modeling and Technology, The American Ceramic Society, 2015.
- [6] K.M. Grant, S. Krämer, J.P.A. Löfvander, C.G. Levi, CMAS degradation of environmental barrier coatings, Surf. Coat. Technol. 202(4) (2007) 653-657.
- [7] K.N. Lee, D.S. Fox, J.I. Eldridge, D. Zhu, R.C. Robinson, N.P. Bansal, R.A. Miller, Upper Temperature Limit of Environmental Barrier Coatings Based on Mullite and BSAS, J. Am. Ceram. Soc. 86(8) (2003) 1299-1306.
- [8] K.N. Lee, D.S. Fox, N.P. Bansal, Rare earth silicate environmental barrier coatings for SiC/SiC composites and Si<sub>3</sub>N<sub>4</sub> ceramics, J. Eur. Ceram. Soc. 25(10) (2005) 1705-1715.
- [9] B.T. Richards, K.A. Young, F. de Francqueville, S. Sehr, M.R. Begley, H.N.G. Wadley, Response of ytterbium disilicate—silicon environmental barrier coatings to thermal cycling in water vapor, Acta Mater. 106 (2016) 1-14.
- [10] E.J. Opila, Oxidation and Volatilization of Silica Formers in Water Vapor, J. Am. Ceram. Soc. 86(8) (2003) 1238-1248.
- [11] B.T. Richards, M.R. Begley, H.N.G. Wadley, Mechanisms of Ytterbium Monosilicate/Mullite/Silicon Coating Failure During Thermal Cycling in Water Vapor, J. Am. Ceram. Soc. 98(12) (2015) 4066-4075.
- [12] D.E. Damby, E.W. Llewellin, C.J. Horwell, B.J. Williamson, J. Najorka, G. Cressey, M. Carpenter, The  $\alpha$ - $\beta$  phase transition in volcanic cristobalite, J. Appl. Crystallogr. 47(Pt 4) (2014) 1205-1215.
- [13] B.J. Harder, Oxidation performance of Si-HfO2 environmental barrier coating bond coats deposited via plasma spray-physical vapor deposition, Surf. Coat. Technol. 384 (2020) 125311.
- [14] Z. Ding, M. Ridley, J. Deijkers, N. Liu, M.S.B. Hoque, J. Gaskins, M. Zebarjadi, P. Hopkins, H. Wadley, E. Opila, K. Esfarjani, The thermal and mechanical properties of hafnium orthosilicate: experiments and first-principles calculations, Materialia (2020) 100793.
- [15] R. Anton, V. Leisner, P. Watermeyer, M. Engstler, U. Schulz, Hafnia-doped silicon bond coats manufactured by PVD for SiC/SiC CMCs, Acta Mater. 183 (2020) 471-483.
- [16] B. Mainzer, R. Jemmali, M. Friess, D. Koch, Microstructural and Mechanical Characterization of Damage Tolerant SiC/SiCN Ceramic Matrix Composites Manufactured Via

- PIP Process, in: D. Singh, M. Fukushima, Y. Kim, K. Shimamura, N. Imanaka, J. T. Ohji, A.a.M. Lanagan (Eds.), Proceedings of the 12th Pacific Rim Conference on Ceramic and Glass Technology2018, pp. 129-135.
- [17] G.W. Brindley, The effect of grain or particle Size on x-ray reflections from mixed powders and alloys, considered in relation to the quantitative determination of crystalline substances by x-ray methods, The London, Edinburgh, and Dublin Philosophical Magazine and Journal of Science 36(256) (1945) 347-369.
- [18] D. Shin, R. Arróyave, Z.-K. Liu, Thermodynamic modeling of the Hf–Si–O system, Calphad 30(4) (2006) 375-386.
- [19] X. Luo, W. Zhou, S.V. Ushakov, A. Navrotsky, A.A. Demkov, Monoclinic to tetragonal transformations in hafnia and zirconia: A combined calorimetric and density functional study, Physical Review B 80(13) (2009) 134119.
- [20] B. Bondars, G. Heidemane, J. Grabis, K. Laschke, H. Boysen, J. Schneider, F. Frey, Powder diffraction investigations of plasma sprayed zirconia, Journal of Materials Science 30(6) (1995) 1621-1625.
- [21] Z. Ji, J.A. Haynes, M.K. Ferber, J.M. Rigsbee, Metastable tetragonal zirconia formation and transformation in reactively sputter deposited zirconia coatings, Surf. Coat. Technol. 135(2) (2001) 109-117.
- [22] X. Zhou, V. Shukla, W.R. Cannon, B.H. Kear, Metastable Phase Formation in Plasma-Sprayed ZrO2 (Y2O3)–Al2O3, J. Am. Ceram. Soc. 86(8) (2003) 1415-1420.
- [23] F. Tarasi, M. Medraj, A. Dolatabadi, J. Oberste-Berghaus, C. Moreau, Amorphous and crystalline phase formation during suspension plasma spraying of the alumina–zirconia composite, J. Eur. Ceram. Soc. 31(15) (2011) 2903-2913.
- [24] M. Amberg, J.R. Günter, Metastable cubic and tetragonal zirconium dioxide, prepared by thermal oxidation of the dichalcogenides, Solid State Ionics 84(3) (1996) 313-321.
- [25] G. Dell'Agli, C. Ferone, G. Mascolo, M. Pansini, Crystallization of monoclinic zirconia from metastable phases, Solid State Ionics 127(3) (2000) 223-230.
- [26] R. Srinivasan, B.H. Davis, Zirconia: A Review of a Super Ceramic, in: D.L. Perry (Ed.), Materials Synthesis and Characterization, Springer US, Boston, MA, 1997, pp. 147-188.
- [27] T. Tsunoura, Y. Okubo, K. Yoshida, T. Yano, T. Aoki, T. Ogasawara, Oxidation behavior of monolithic HfSi<sub>2</sub> and SiC fiber-reinforced composites fabricated by melt infiltration using Si-8.5 at%Hf alloy at 800-1200°C in dry air, J. Ceram. Soc. Jpn. 126(1) (2018) 27-33.
- [28] K.J. Hubbard, D.G. Schlom, Thermodynamic stability of binary oxides in contact with silicon, J. Mater. Res. 11(11) (1996) 2757-2776.
- [29] D.G. Schlom, C.A. Billman, J.H. Haeni, J. Lettieri, P.H. Tan, R.R.M. Held, S. Völk, K.J. Hubbard, High-K Candidates for Use as the Gate Dielectric in Silicon Mosfets, Thin Films and Heterostructures for Oxide Electronics, Springer US, Boston, MA, 2005, pp. 31-78.
- [30] D. Shin, Z.-K. Liu, Phase stability of hafnium oxide and zirconium oxide on silicon substrate, Scripta Mater. 57(3) (2007) 201-204.
- [31] D.-Y. Cho, K.-S. Park, B.-H. Choi, S.-J. Oh, Y.J. Chang, D.H. Kim, T.W. Noh, R. Jung, J.-C. Lee, S.D. Bu, Control of silicidation in HfO2/Si(100) interfaces, Appl. Phys. Lett. 86(4) (2005) 041913.
- [32] H. Takahashi, J. Okabayashi, S. Toyoda, H. Kumigashira, M. Oshima, K. Ikeda, G.L. Liu, Z. Liu, K. Usuda, Annealing-time dependence in interfacial reaction between poly-Si electrode and HfO2/Si gate stack studied by synchrotron radiation photoemission and x-ray absorption spectroscopy, Appl. Phys. Lett. 89(1) (2006) 012102.
- [33] D.-Y. Cho, S.-J. Oh, Y.J. Chang, T.W. Noh, R. Jung, J.-C. Lee, Role of oxygen vacancy in HfO2/SiO2/Si(100) interfaces, Appl. Phys. Lett. 88(19) (2006) 193502.
- [34] S. Stemmer, Thermodynamic Considerations in the Stability of Binary Oxides for Alternative Gate Dielectrics in CMOS, Journal of Vacuum Science & Technology B 22(2) (2004).

- [35] C.M. Perkins, B.B. Triplett, P.C. McIntyre, K.C. Saraswat, E. Shero, Thermal stability of polycrystalline silicon electrodes on ZrO2 gate dielectrics, Appl. Phys. Lett. 81(8) (2002) 1417-1419.
- [36] P. Kalita, S. Saini, P. Rajput, S.N. Jha, D. Bhattacharyya, S. Ojha, D.K. Avasthi, S. Bhattacharya, S. Ghosh, Oxygen vacancy mediated cubic phase stabilization at room temperature in pure nano-crystalline zirconia films: a combined experimental and first-principles based investigation, PCCP 21(40) (2019) 22482-22490.
- [37] K. Smits, D. Olsteins, A. Zolotarjovs, K. Laganovska, D. Millers, R. Ignatans, J. Grabis, Doped zirconia phase and luminescence dependence on the nature of charge compensation, Scientific Reports 7(1) (2017) 44453.
- [38] S. Fabris, A.T. Paxton, M.W. Finnis, A stabilization mechanism of zirconia based on oxygen vacancies only, Acta Mater. 50(20) (2002) 5171-5178.
- [39] G.M. Ingo, Origin of Darkening in 8 wt% Yttria—Zirconia Plasma-Sprayed Thermal Barrier Coatings, J. Am. Ceram. Soc. 74(2) (1991) 381-386.
- [40] J.A. Deijkers, H.N.G. Wadley, Hafnium silicate formation during oxidation of a permeable silicon + HfO2 powder composite system, Acta Mater. 201 (2020) 448-461.
- [41] K. Yamahara, K. Okazaki, K. Kawamura, Molecular dynamics study of the thermal behaviour of silica glass/melt and cristobalite, J. Non-Cryst. Solids 291(1) (2001) 32-42.
- [42] L. Huang, J. Kieffer, Structural Origin of Negative Thermal Expansion in High-Temperature Silica Polymorphs, Phys. Rev. Lett. 95(21) (2005) 215901.